Magnetic, transport, and electron magnetic resonance properties of $Pr_{0.8}Ca_{0.2}MnO_3$ single crystals

V. Markovich,[1] I. Fita,[2,3] A. I. Shames,[1] R. Puzniak,[2] E. Rozenberg,[1] C. Martin,[4] A. Wisniewski,[2] Y. Yuzhelevskii,[1] A. Wahl,[4] and G. Gorodetsky[1]

[1]*Department of Physics, Ben-Gurion University of the Negev, 84105 Beer-Sheva, Israel*
[2]*Institute of Physics, Polish Academy of Sciences, 02-668 Warsaw, Poland*
[3]*Donetsk Institute for Physics and Technology, National Academy of Sciences, R. Luxemburg Street 72, 83114 Donetsk, Ukraine*
[4]*Laboratoire CRISMAT, UMR 6508, ISMRA, 14050 Caen Cedex, France*

Magnetic, transport, and electron magnetic resonance properties of $Pr_{0.8}Ca_{0.2}MnO_3$ single crystals have been investigated. Two ferromagnetic transitions observed at $T_{C1} \approx 130$ K and $T_{C2} \approx 60$ K, denote a long range ordering of Mn and Pr spins, respectively, and exhibit an opposite pressure coefficient for T_C, $dT_{C1}/dP \approx 0.24$ K/kbar and $dT_{C2}/dP \approx -0.75$ K/kbar, respectively. The angular dependence of the magnetization in the (100) plane shows a strong twofold anisotropy, which increases under pressure. It was found that the resistivity $\rho(T)$ obeys the Arrhenius law at 140 K $\leq T \leq 300$ K with an activation energy $E_a = 130$ meV, whereas below T_{C1}, $E_a = 60$ meV. The dynamic magnetoresistance vs magnetic field approaches a highest value of about 25% near T_{C1} for $H = 14.5$ kOe. The dynamic resistance R_d exhibits a pronounced dependence on a bias current I at $T < T_{C1}$. The results can be explained by the formation of orbital ordered states, which give rise to anisotropy and localization in the ferromagnetic insulating matrix. Electron magnetic resonance reveals coexistence of ferromagnetic metallic and insulating phases just below T_{C1}. The signal of the metallic phase sharply drops in intensity at decreasing temperature. This effect is attributed to the formation of spin/cluster glass state. Possible mechanisms of current induced suppression of dynamic resistance in the ferromagnetic state are also discussed.

I. INTRODUCTION

The observation of colossal magnetoresistance (CMR) in hole-doped perovskite-type manganites $L_{1-x}A_xMnO_3$ (L = trivalent lanthanide ion; A = alkaline metal) has promoted extensive studies of these compounds, in recent years.[1,2] Manganites were found to exhibit a plethora of magnetic and electronic phases, depending on the value of the doping x and the averaged A site cation radius $\langle r_A \rangle$. It is widely accepted that the predominant CMR mechanism arises mainly due to the double exchange (DE) interaction mediated by hopping of spin-polarized e_g electrons, between Mn^{3+} and Mn^{4+}, thereby facilitating both the electrical conductance and the ferromagnetic (FM) coupling in the ferromagnetic metallic (FMM) phase. On the other hand, certain electron orbital configurations energetically favor superexchange (SE) interactions between localized electrons and may yield a formation of ferromagnetic insulating (FMI) or antiferromagnetic (AFM) phases.[3] Special attention in this regard was given to the Jahn-Teller (JT) effect. Millis *et al.*[4] claimed that the double exchange alone cannot explain CMR and the resistivity peak in the vicinity of Curie temperature T_C. They proposed that JT interactions should also be taken into account. According to recent studies the ground states of some manganites exhibit a strong tendency toward phase separation (PS) involving phases with different magnetic and orbital/charge ordering.[2]

Among the variety of hole-doped manganese perovskites, the $Pr_{1-x}Ca_xMnO_3$ (PCMO) is of special interest for the following reasons. (i) The similarity in the size of Ca^{2+} and Pr^{3+} cations establishes a situation for which $\langle r_A \rangle$ is practically constant (1.18 Å) and there is a very low mismatch

whatever x is.[5] (ii) The compounds exhibit insulating behavior over the entire composition range because of the narrow bandwidth of the e_g electrons and the corresponding weak DE interaction.[5,6] In the intermediate region $0.3 < x < 0.8$ the PCMO system undergoes a charge ordering (CO) transition and AFM ordering of Mn^{3+} and Mn^{4+} at Néel temperatures: $T_N \approx 170$ K for $x = 0.3$ and $T_N \approx 100$ K for $x = 0.8$.[5,6] The charge ordered state in PCMO systems is very sensitive to different external "perturbations." For example, it may be destabilized upon application of x-ray,[7] light,[8,9] external pressure,[10] or electric field/current.[11] According to the existing phase diagram[5,6] of the low doping range ($0.1 < x < 0.3$) PCMO represents a pure FMI phase in its ground state. For $x = 0.2$ a robust ferromagnetism with magnetic moment of $4\,\mu_B$/f.u. was found at a temperature of $T = 5$ K and magnetic field of 25 kOe.[5,12] Exotic effects[13,14] of current-driven magnetization changes were also found in $Pr_{0.8}Ca_{0.2}MnO_3$ single crystal.

The aim of this paper is to report on experimental investigations that reveal some of the specific features of magnetic and transport properties of $Pr_{0.8}Ca_{0.2}MnO_3$ single crystal and provide some experimental evidences for phase separation. The experiments involve measurements of magnetization at various pressures as well as dc and dynamic resistance and electron magnetic resonance (EMR).

II. EXPERIMENT

The $Pr_{0.8}Ca_{0.2}MnO_3$ crystal was grown by a floating zone method using an image furnace.[13] More details, including results of x-ray diffraction and electron diffraction as well as neutron diffraction studies are presented elsewhere.[12,13] The

unit cell of this crystal is orthorhombic having a P_{nma} space group.[13] A crystal for the resistivity measurements was prepared in the form $(5 \times 2 \times 1.6)$ mm^3 having its longest dimension along $\langle 100 \rangle$ orthorhombic direction. Evaporated silver strips with a separation of about 0.5 mm between the voltage (V) contacts were used for the customary four-point resistance measurements. ac measurements of dynamic resistance ($R_d = dV/dI$) were performed using a lock-in technique and a modulation current 5 μA at 390 Hz. For the measurements of R_d vs bias current, the applied current I was limited to avoid any heating of the sample. Measurements of dynamic magnetoresistance $R_d(H)$ were carried out in a longitudinal geometry for which magnetic fields H up to 15 kOe was aligned parallel to the current direction. Magnetization measurements were performed at various temperatures and magnetic field up to 50 kOe by using a superconducting quantum interference device (SQUID) magnetometer. A cylinder-shape sample having a diameter of 1 mm and height of 4.0 mm with $\langle 100 \rangle$ axis of rotation was used for measurements of magnetization under hydrostatic pressure. The measurements were performed in the temperature range 4.2–220 K and magnetic fields up to 15 kOe, using PAR (Model 4500) vibrating sample magnetometer. Details of the magnetic measurements under pressure are presented elsewhere.[15]

Electron magnetic resonance (EMR) measurements, namely, ferromagnetic resonance (FMR) at $T < T_C$ and electron paramagnetic resonance (EPR) at $T > T_C$ were carried out using Bruker EMX-220 X band ($\nu = 9.4$ GHz) spectrometer within the temperature range 116 K $\leqslant T \leqslant$ 460 K. For a detailed description of the method of measurements, see Ref. 16. All measurements were performed on a loose-packed micron-sized (5–20 μm) crushed crystal. The reasons for selecting such a sample for our EMR measurements are described in detail in Ref. 17.

III. RESULTS

A. Magnetic properties

Figure 1(a) presents field cooled (FC) and zero field cooled (ZFC) magnetization curves (M_{FC} and M_{ZFC}, respectively), for H aligned along the easy direction in the (100) plane. The abrupt change in the magnetization at about $T \approx 130$ K is attributed to magnetic ordering of the Mn sublattice. The slight change in the slope of M_{FC} and M_{ZFC} curves is attributed to the ordering of Pr moments. Such a low temperature ordering of Pr moments at $T \approx 60$ K is a characteristic feature of the PCMO system.[6,12,18] The ferromagnetic transition temperature of the Mn spins T_{C1} at various pressures was determined by maximal slope in both $M_{FC}(T)$ and $M_{ZFC}(T)$ dependences. The results as well as the pressure dependence of the ordering temperature of Pr spins T_{C2} are shown in Fig. 1(b). The observed pressure coefficient of the two transition temperatures are remarkably different: $dT_{C1}/dP \approx 0.24$ K/kbar and for $dT_{C2}/dP \approx -0.75$ K/kbar; see Fig. 1(b). It shoud be noted that at higher pressures the change in the slopes of the magnetization curves at T_{C2} is much less pronounced and this hampers the determination of T_{C2} and dT_{C2}/dP as well.
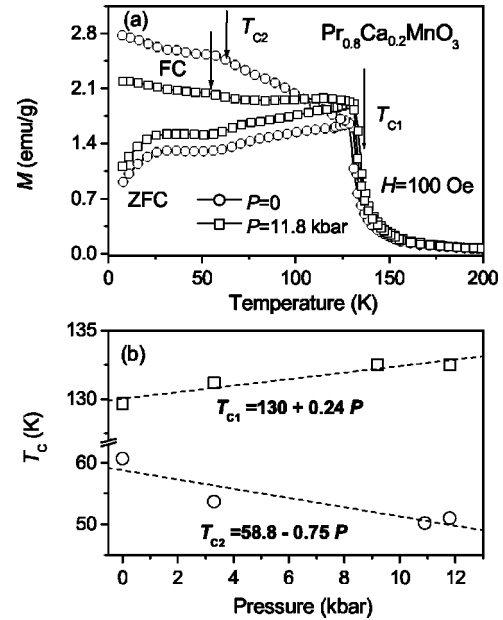
FIG. 1. (a) Field cooled (M_{FC}) and zero field cooled (M_{ZFC}) magnetization measured at applied magnetic field $H = 100$ Oe applied along easy axis in (100) plane, for $P = 0$ and $P = 11.8$ kbar. T_{C1} and T_{C2} denote the ferromagnetic transition temperatures of Mn and Pr spins, respectively. (b) Pressure dependence of the ferromagnetic transition temperatures T_{C1} and T_{C2}. The dashed lines are linear fits.

Magnetization curves M vs magnetic field H for various temperatures at ambient pressure along the easy direction $\langle 100 \rangle$ were measured. A relatively high magnetic field (of about 5 kOe) is required to saturate the magnetization at $T = 5$ K. The high value of saturated magnetization obtained is found to be in compliance with neutron diffraction[18] measurements, which show that both the Mn and Pr are aligned along $\langle 100 \rangle$ at $T < T_{C2}$. The nature of the magnetic anisotropy in (100) plane is seen in Fig. 2. It presents the angular dependence of the magnetization in this plane for an applied magnetic field of $H = 10$ kOe, at various temperatures. A
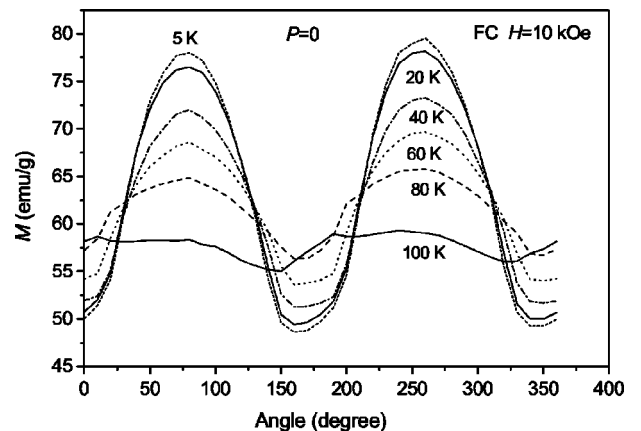
FIG. 2. The angular variation of the magnetization of the $Pr_{0.8}Ca_{0.2}MnO_3$ single crystal in (100) plane at various temperatures at $P = 0$ under magnetic field $H = 10$ kOe.
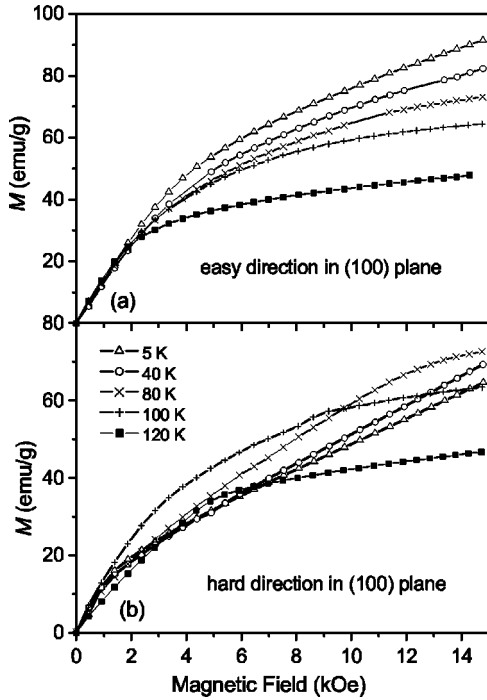
FIG. 3. Magnetization curves M vs H of the $Pr_{0.8}Ca_{0.2}MnO_3$ crystal measured at $P=0$ for various temperatures. The magnetic field is applied along (a) easy and (b) hard directions in the (100) plane.

twofold symmetry for $M(\theta)$ is clearly observed below $T = 80$ K, suggesting an uniaxial magnetocrystalline anisotropy of the form $K \sin 2\theta$. Here, K is anisotropy constant and θ, is the angle that the magnetic field H forms with the local easy axis in (100) plane. A similar kind of anisotropy was observed earlier in (100) plane of low doped $La_{1-x}Ca_xMnO_3$ ($x=0.18$, 0.2, 0.22).[15,17] Measurements of $M(H)$ were carried out for H aligned along the easy and hard directions in (100) plane, at various temperatures, see Figs. 3(a), 3(b). One should noted in Fig. 3(b), that $\Delta M(H)/\Delta H$ at low fields does not monotonically increase for decreasing temperature, as observed for easy direction [see Fig. 3(a)].

In contrary to the pronounced suppression of magnetic anisotropy obtained for $La_{1-x}Ca_xMnO_3$ ($x=0.18$, 0.2, 0.22) under pressure,[15,17] $M(H)$ of $Pr_{0.8}Ca_{0.2}MnO_3$ measured along the easy and hard directions in (100) plane show a pronounced increase of magnetic anisotropy at $T<100$ K under pressure. The effective anisotropy fields H_A in (100) plane at ambient pressure and $P=10.9$ kbar are given in Fig. 4(a). We have also drawn the dimensionless parameter $(M_{\max}-M_{\min})/M_{\min}$ using maximal and minimal values of angular dependences of magnetization in (100) plane at ambient pressure and at $P=10.9$ kbar [Fig. 4(b)] for the entire temperature range $T<T_{C1}$. Magnetization loops at $T=5$ K (not shown) along easy and hard directions in (100) plane exhibit a ferromagnetism with distinct differences related to the local easy and hard directions and a coercive field of about few hundreds of Oe.

B. Resistance and magnetoresistance

Figure 5 presents the temperature dependence of the resistivity $\rho(T)$ in a semilogarithmic scale, for various electric
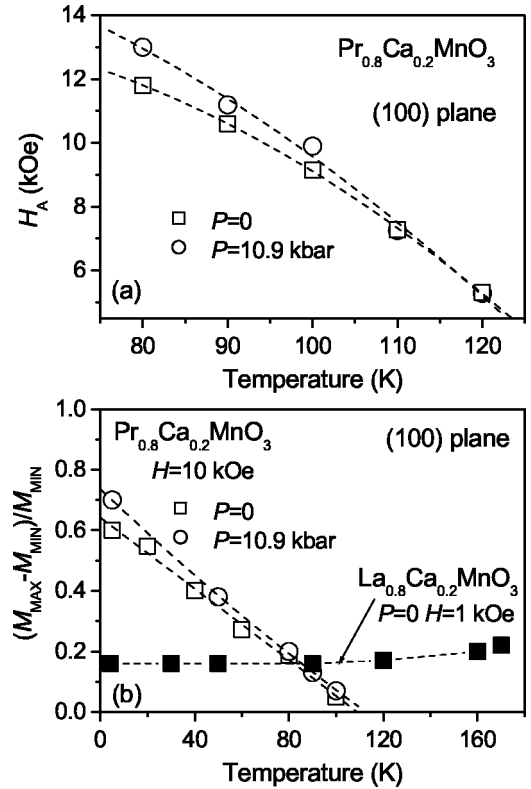
FIG. 4. (a) Temperature dependence of the magnetic anisotropy field H_A in the (100) plane. (b) Dimensionless parameter $(M_{\max}-M_{\min})/M_{\min}$ of $Pr_{0.8}Ca_{0.2}MnO_3$ single crystal. The temperature evolution of the parameter $(M_{\max}-M_{\min})/M_{\min}$ for the $La_{0.8}Ca_{0.2}MnO_3$ crystal measured at $P=0$ and $H=1$ kOe (Ref. 15) is also presented. Dashed lines are guide to the eyes.

currents $I=5$, 50, 100 μA, upon cooling. At temperatures higher than T_{C1}, the resistivity obeys Arrhenius law of the form $\rho(T)=\rho_0 \exp(E_a/kT)$ with an activation energy $E_a=0.13\pm0.005$ eV. This is found in a qualitative agreement with the results of Jirak et al.[6] It should be emphasized that ρ vs T^{-1} for different currents practically coincide at temperatures above T_{C1}. Below T_{C1} the resistivity becomes current
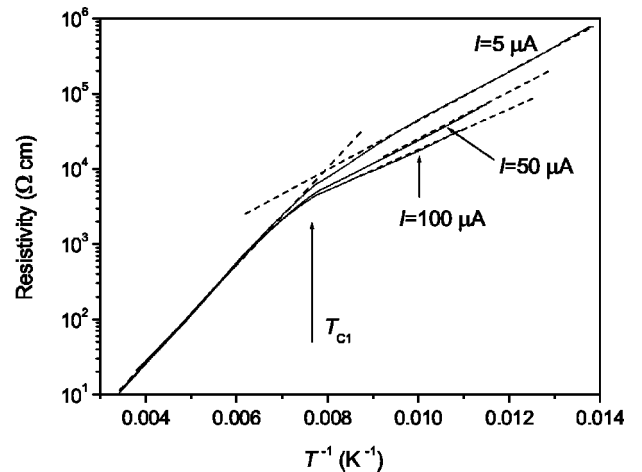
FIG. 5. The resistivity of the $Pr_{0.8}Ca_{0.2}MnO_3$ single crystals as a function of temperature. The dashed lines are guides to the eyes.
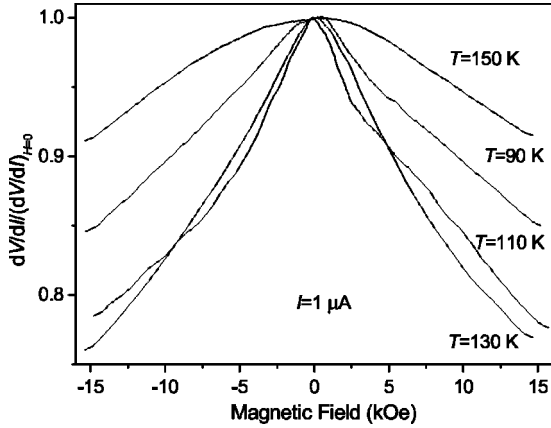
FIG. 6. Magnetic field dependence of the dynamic resistivity of the $Pr_{0.8}Ca_{0.2}MnO_3$ single crystal at various temperatures.

dependent and the curves changes their initial slope, see Fig. 5. They obey Arrhenius law with activation energy $E_a \approx 0.06 \pm 0.005$ eV.

Measurements of the dynamic resistance R_d at various magnetic fields or for various bias currents I were performed as a part of electrical transport studies. The effect of magnetic fields up to 15 kOe on R_d at various temperatures is seen in Fig. 6. At room temperature $R_d(H)$ is practically constant (not shown), whereas for temperatures approaching T_{C1} from above a bell shape form of $R_d(H)$ was observed. At temperatures $T \lesssim T_{C1}$ the dynamic resistance R_d vs H is nearly linear, see Fig. 6. A maximal effect of about 25% is observed near T_{C1}. Figure 7 displays R_d of $Pr_{0.8}Ca_{0.2}MnO_3$ crystal at various temperatures as a function of the current flow. Small effects of current or magnetic field on R_d were observed even at temperatures much higher than T_{C1}, see
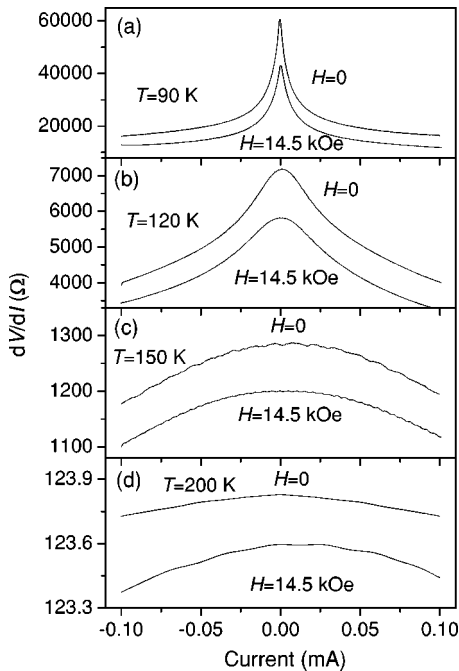
FIG. 7. Dynamic resistivity of the $Pr_{0.8}Ca_{0.2}MnO_3$ single crystal vs current at various temperatures.
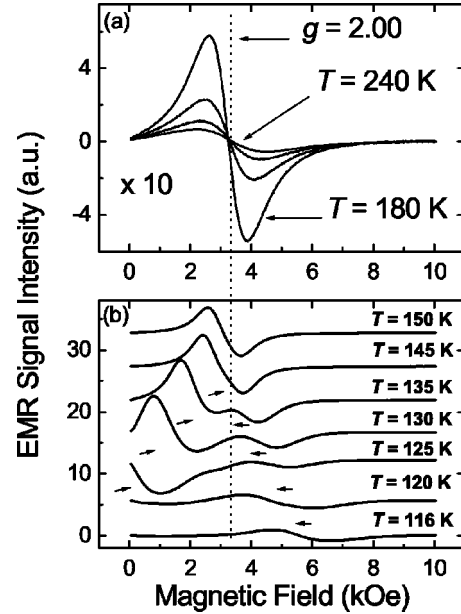
FIG. 8. Temperature dependence of EMR spectra of loose-packed $Pr_{0.8}Ca_{0.2}MnO_3$ sample, $\nu = 9.434$ GHz: (a) PM region, (b) FM region, the arrows point out the shift of the corresponding EMR lines towards $g = 2.00$ position (vertical dashed line) at temperatures approaching T_{C1}.

Fig. 7(d). Such an effect with a bell-shape current dependence becomes more pronounced as the temperature approaches T_{C1} from above [Fig. 7(c)]. Below T_{C1} the effect of current increases strikingly with decreasing temperature; see Figs. 7(a), 7(b).

C. Electron magnetic resonance

EMR spectra (Fig. 8) of the loose-packed sample demonstrate a complex structure at temperatures approaching T_{C1} from below. Namely, starting at $T = 116$ K, a Gaussian-shaped resonance line of $H_r \cong 5.5$ kOe and width $\Delta H_{pp} \cong 1.89$ kOe is superimposed onto the negative shoulder of a weak broad line, centered at zero field. With heating both lines become narrower and shift towards a magnetic field value corresponding to $g \sim 2$; see Figs. 8(b) and 9. At $T > 120$ K the low field resonant line becomes well defined. The above two lines merge to a single one in the vicinity of $T_{C1} = 130$ K, but the second derivative EMR spectra enables one to distinguish them up to $T \sim 145$ K, see Fig. 8(a). Moreover, the discussed lines converges into a Lorentzian shaped one only at temperatures above $T = 160$ K.

The temperature dependence of the double integrated intensity (DIN) of the EMR spectra is plotted in Fig. 10(a). Within the FM region, the DIN value exhibits a significant enhancement at $T_{max} = 132.5$ K and then abruptly drops with decreasing temperature. In the paramagnetic (PM) region ($T > T_{C1}$), the intensity of the EMR line obeys an approximate Curie-Weiss behavior with $\theta \sim 200$ K. The Arrhenius plot of DIN clearly shows two linear segments—see Fig. 10(b)—that may be well fitted with activation energies $\Delta E_a^1 = 99 \pm 1$ meV (130 K $< T <$ 200 K) and $\Delta E_a^2 = 71$
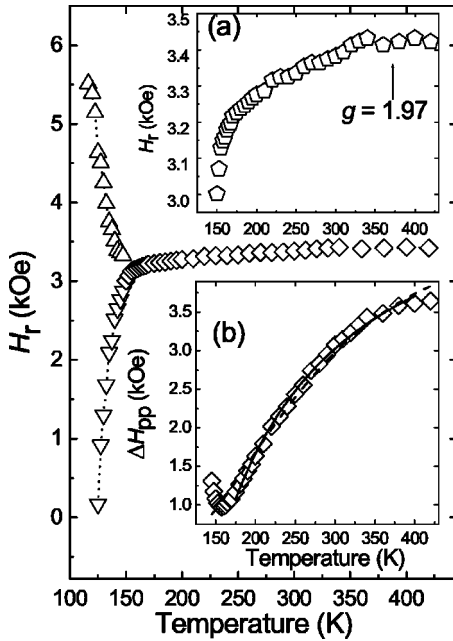
FIG. 9. Temperature dependence of resonance fields H_r for $Pr_{0.8}Ca_{0.2}MnO_3$: triangles up—signal ascribed to the FMI phase; triangles down—signal ascribed to the FMM phase; diamonds—the PM phase signal. Dashed lines are guides to the eyes. (a) A zoom of $H_r(T)$ for the PM signal. (b) Temperature dependence of the line width ΔH_{pp} above T_{C1}: dashed line—best fit according to the model of Shengelaya et al. (Ref. 20), solid line—best fit according to the Huber's model (Ref. 21).

FIG. 10. (a) Temperature dependences of double integrated intensity DIN for $Pr_{0.8}Ca_{0.2}MnO_3$. (b) Arrhenius plot of DIN, the solid and dashed lines represent the best linear fits above and below $T=200$ K, respectively.

± 1 meV (200 K$<T<$420 K). The physical meaning of ΔE_a has been discussed in Ref. 19 in which the constant coupling approximation (CCA) model of resonating centers describes a progressive clustering of the Mn^{3+}-Mn^{4+} ions mediated by the hopping of electrons. Even within the PM region the EMR line continues shifting to higher fields reaching the resonance field (H_r) corresponding to $g=1.97$ ± 0.01 at $T>300$ K [see Fig. 9(a)]. The $\Delta H_{pp}(T)$ dependence for this line shows a minimum at $T_{min}=157.5$ K [see Fig. 9(b)]. It is shown here that both the "bottleneck" model[20] and the Huber's model[21] may describe the $\Delta H_{pp}(T)$ dependence quite satisfactorily. A least square fit of the "bottleneck" model [see Fig. 9(b), dashed line] provides us with the value of $\Delta E_a^\sigma = 56 \pm 3$ meV and $\Delta H_{pp}^0 = 330$ ± 130 Oe, whereas Huber's model (ibid, solid line) yields $\Delta H_{pp}(\infty) = 5760 \pm 50$ Oe and $\theta_{PM} = 142 \pm 1$ K.

IV. DISCUSSION

The nature of the FMI ground state of PCMO system at $x<0.3$ is a subject of many discussions in recent years. Some of the intriguing properties of these compounds were attributed to an orbital polaron lattice characterized by polaron-type charge and orbital ordering (OO).[22] On the other hand, recent x-ray resonant scattering studies for $x=0.25$ show that only long-range orbital ordering occurs with no indication of CO.[23] Though, the pressure effect on T_C and FM interactions was extensively studied in the past for various manganite

systems (Refs. 2, 15, 17, and references therein), no studies, to the best of our knowledge, of the FMI ground state (0.1 $<x<0.3$) of PCMO under pressure have ever been reported. According to our experimental results, the pressure dependences of both transition temperatures T_{C1} and T_{C2} are linear, see Fig. 1(b). The pressure coefficient of T_{C1} matches with that of T_C for $La_{0.8}Ca_{0.2}MnO_3$ and $La_{0.82}Ca_{0.18}MnO_3$ and significantly differs from that of $La_{0.78}Ca_{0.22}MnO_3$.[17] The similarity in the pressure coefficient may be attributed to the dominant ferromagnetic SE interactions in FMI ground state, existing in these compounds. In the case of $La_{0.78}Ca_{0.22}MnO_3$, the DE is a significant exchange and it has much higher sensitivity to pressure.[15]

The magnetization measured at $T=5$ K along $\langle 100 \rangle$ approaches a value higher than $4 \mu_B$/f.u. in magnetic field H >20 kOe. This value is higher than that expected for the magnetic moment of Mn spins alone. For the present ratio of Mn^{3+} and Mn^{4+} one expects to get $3.8\mu_B$/f.u. The comparison of $M(H)$ dependences for different directions shows that the $\langle 100 \rangle$ direction is an easy direction for both Mn and Pr moments, in compliance with previous results of magnetization[5,12] and neutron diffraction.[6,18] The FM ordering of Pr moments may arise due to the exchange coupling between localized $4f$ spins of Pr ions and neighboring Mn spins. Correlating the magnetic measurements with the neutron diffraction[16] measurements, one may conclude that the ferromagnetic ordering of the Pr^{3+} spins manifests itself by a change in the slope of the magnetization (see Fig. 1) and the magnetic susceptibility.[12] The superexchange interaction between Pr ions and neighboring Mn ions depends on the charge, crystallographic structures, and the relative orientation of the corresponding orbitals.

It is of interest to compare the magnetic anisotropy of $Pr_{0.8}Ca_{0.2}MnO_3$ with that previously reported for $La_{1-x}Ca_xMnO_3$.[15,17] (i) The magnetic anisotropy of $Pr_{0.8}Ca_{0.2}MnO_3$ is found to be much higher and increases with decreasing temperature and at applied pressure, while in the case of $La_{0.8}Ca_{0.2}MnO_3$ an applied pressure suppresses strongly the magnetic anisotropy in the (100) plane.[15] (ii) The value of $(M_{max}-M_{min})/M_{min}$ for $La_{0.8}Ca_{0.2}MnO_3$ exhibits other trend at low temperatures (see Fig. 4—the data of the magnetization were taken from Ref. 15). The angular dependence of the magnetization of $La_{0.8}Ca_{0.2}MnO_3$ (Ref. 15) was measured in a magnetic field of $H=1$ kOe, because magnetic fields of ~ 10 kOe suppress completely such a dependence. The much stronger anisotropy of the magnetic interaction in (100) plane found in $Pr_{0.8}Ca_{0.2}MnO_3$ may be attributed to the more pronounced orthorhombic distortions in PCMO in comparison to $La_{1-x}Ca_xMnO_3$ lattices. The spontaneous orthorhombic strain defined by $s=2(b-a)/(b+a)$, is $s=0.0377$ and $s=0.0646$ at room temperature for parent compounds $LaMnO_3$ and $PrMnO_3$,[24] respectively. Higher lattice distortions in $PrMnO_3$ in so-called O' orthorhombic structure ($c/\sqrt{2}<a<b$), are characterized by stronger JT interactions and higher Jahn-Teller (T_{JT}) transition temperatures, respectively. In fact, the parent compound $LaMnO_3$ undergoes a structural phase transition at $T_{JT} \approx 750$ K,[25] above which the OO disappears. For $PrMnO_3$ a similar transition takes place at about 1050 K.[26] The evaluation of s for $La_{1-x}Ca_xMnO_3$ crystals[15,17] shows that it ranges from $s=0.0014$ for $x=0.18$ to $s=0.00001$ for $x=0.22$ and these crystals belong rather to a quasicubic phase O'^* ($c/\sqrt{2}\sim a\sim b$). On the other hand, the value of s for $Pr_{0.8}Ca_{0.2}MnO_3$ (Refs. 5, 18) is 0.0206 at room temperature and $s=0.0233$ at $T=10$ K. This means that at this level of the Ca doping a strong enough orthorhombic distortions of perovskite structure still retain. Using the local-spin-density approximation method Solovyev *et al.*[27] have shown that JT lattice distortions play a crucial role in the formation of magnetocrystalline anisotropy, as well as in the anisotropic and isotropic exchange interactions of perovskite manganites. In PCMO the Pr moments couple with Mn spins and may be very essential to the physical properties at low temperatures. It was suggested[28] that Pr spins dominate the low temperature thermodynamics of $Pr_{0.7}Ca_{0.3}MnO_3$ and exhibits a soft spin wave spectrum relative to other FM perovskite manganites. The very low values of spin-wave stiffness D were observed in $Pr_{0.7}Ca_{0.3}MnO_3$,[28] $D\approx 25\pm 2$ meV $Å^2$ and $Pr_{0.8}Ca_{0.2}MnO_3$,[12] $D\approx 15\pm 3$ meV $Å^2$. It is supposed that the coupling between the Mn and the Pr moments having an easy axis along $\langle 100 \rangle$ direction leads to an increment of the magnetic anisotropy at $T<T_{C2}$, see Fig. 4.

As noted previously, the resistivity shows an insulating behavior in the whole temperature range of our measurements, though a marked drop in the activation energy is seen below T_{C1}, see Fig. 5. Such a behavior is a characteristic feature of magnetic semiconductors, where the activation energy depends strongly on the long-range magnetic order.[29] Additional source for such drop in the E_a may presumably be associated with anomalies of the a and b lattice parameters in the vicinity of T_{C1},[18] yielding a modification in the phonon spectrum and band structure. Particularly, ferromagnetic transition at T_{C1} is accompanied not only by a drop of a lattice parameter, but also by a change in the temperature variation of the orthorhombic strain parameter s. From the temperature dependence of the lattice parameters,[18] one may conclude that s increases upon lowering the temperature from 300 to about 150 K, while it slightly decreases upon decreasing temperatures at $T<T_{C1}$. It should be noted that at low temperatures $T<70$ K in small bias currents (<1 mA) the resistivity of $Pr_{0.8}Ca_{0.2}MnO_3$ is too high to be measured, see Fig. 5 and Ref. 13. For higher bias currents (>10 mA) the resistance of $Pr_{0.8}Ca_{0.2}MnO_3$ crystal is strongly depressed and saturates at decreasing temperature.[13] At these currents a slight anomaly of the resistivity $R(T)$ was observed around 50 K, presumably linked to the ferromagnetic Pr ordering.[13] In inhomogeneous materials, because of the rather random distribution of Mn^{3+} and Mn^{4+} ions, the DE operates in spatially distinct disordered regions of the sample. These regions with mobile carriers at decreasing temperature are more and more interrupted by tunnel-type weak links associated with twin boundaries of single crystalline sample[13,30] and the Pr ordering will only slightly affect the tunneling conductivity.

The dynamic resistance R_d exhibits a negative magnetoresistance (MR) effect, a characteristic feature of magnetic semiconductors, where the band structure is spin dependent and two subbands are found for the majority (spin directed parallel to the magnetization) and minority (spin antiparallel to the magnetization) carriers. A magnetic field pushes down the bottom of the spin-up subband and as a consequence the gap between conduction and valence bands decreases, resulting in a lowering of resistance. In low doped $La_{1-x}Ca_xMnO_3$ ($x=0.18$, 0.2) and in the range of moderate magnetic field (up to 10 kOe) a positive MR was observed[15,17] below T_C. This effect may occur only in a predominantly FMI ground state with SE interactions. Negative magnetoresistance is rather a hallmark of the DE interactions in manganites and presumably reflects the presence of FMM regions in the predominantly ferromagnetic insulating matrix of a $Pr_{0.8}Ca_{0.2}MnO_3$ sample.

Modest electric current/field applied to charge-ordered manganites may lead to a metal-insulator transition and a prominent nonlinearity of voltage-current characteristics. In the case of the FMI ground state the nature of the interaction between current and magnetic moments may be much more complicated. An applied current may affect the dynamic resistance R_d, and in our case such an effect increases strongly with decreasing temperature, see Figs. 5, 7. Let us discuss the possible reasons of such a behavior. Orbital ordering may give rise not only to magnetic anisotropy of $Pr_{0.8}Ca_{0.2}MnO_3$ but also to a strong localization effect. An electric current/field may thus induce a local electrical moment in MnO_6 octahedra by modifying the spatial distribution of their charges and suppressing the JT local distortion, thereby leading to delocalization effects. According to Tokura and Nagaosa[31] the electric field may directly affect the directional order of the orbital, when the compound is insulating enough, and alter the magnetic state. Such features were ob-

served in $Pr_{0.8}Ca_{0.2}MnO_3$ crystal in the present work and also in Refs. 13, 14. Another mechanism for current driven suppression of resistivity may be associated with condensate effects of charge density waves (CDW's) or spin density waves (SDW's). Recently, Kida and Tonouchi[32] have found spectroscopic evidence of CDW condensate in charge-ordered $Pr_{0.7}Ca_{0.3}MnO_3$, which arises due to quasi-one-dimensional CO and OO. A characteristic feature of CDW systems is a rising of nonlinear conduction and sudden motion of CDW (CDW depinning),[33] when electric current/field exceeds some threshold value. Similar behavior was observed[11] for charge ordered $Pr_{1-x}Ca_xMnO_3$ ($0.3 < x < 0.4$) samples. In the case of $Pr_{0.8}Ca_{0.2}MnO_3$, a sharp decrease of the dynamic resistance is seen even for small electric current/field, see Fig. 7. It is worth noting that SDW systems exhibit a much lower spin gap ~ 10 meV, in comparison with CDW systems, where the single-particle excitation is characterized by a gap of ~ 100 meV.[33] Therefore, nonlinear transport in SDW systems may occur at low values of applied current/field. Goodenough[34] has pointed out that for ferromagnetism mediated by SE interactions, the SDW state may be stabilized, if the intraatomic electron-electron interactions are not strong enough to remove completely the spin degeneracy of the band.

EMR spectra of the $Pr_{0.8}Ca_{0.2}MnO_3$ sample clearly demonstrate that the magnetic state is phase separated consisting of two distinguished magnetic phases. Comparing with EMR and $\rho(T)$ data, obtained on a similar $La_{0.82}Ca_{0.18}MnO_3$ sample,[17] one may conclude that the high field EMR signal, observed at $T \geq 116$ K [see Fig. 8(b)] belongs to FMI phase, which exhibits a certain strong magnetocrystalline anisotropy. Another fast growing EMR signal, which shifts from zero fields with increasing temperature and becomes observable at $T > 120$ K, resembles EMR signals previously observed in homogeneous FMM manganites. This signal may be attributed to the FMM phase chracterized by uniaxial magntic anisotropy. It is worth mentioning here that EMR reveals the presence of the PS (FMI+FMM) magnetic state at temperatures up to $\sim 1.1\, T_{C1}$. The asymmetry of EMR signals disappears at $T \sim 1.2\, T_{C1}$. Only above these temperatures can the sample be considered as having no long range magnetic ordering at all. The signal intensity above $1.2\, T_{C1}$ obeys Arrhenius behavior with two different activation energies, alternating at $T \sim 200$ K—see Fig. 10(b). One may assume that at $T \sim 200$ K the magnetic interactions in Mn^{3+}-Mn^{4+} undergo a change. Moreover, the effective g factor of the singlet Lorentzian line, which, far above T_{C1}, indicates the strength of internal magnetic fields acting on the PM entity, starts leveling off above 220 K.

Let us discuss the unusual sharp drop of DIN below T_{max}, where the magnetization saturates rapidly slightly below T_{C1} (see above). The DIN is proportional to the relative amount of the corresponding magnetic phase within the sample's volume and to its high frequency magnetic susceptibility. Therefore, the sharp reduction of DIN by decreasing T may arise because of (a) a reduction in the actual amount of magnetic phase, (b) a shift of the EMR signal towards zero field, i.e., an appearance of a nonresonant FMR microwave

absorption[35] and (c) the formation of so called spin (or cluster) glass state, for which some magnetic moments become "frozen" and "invisible" at higher frequencies, as has been earlier observed by measurements of ac susceptibility.[36] Magnetization data for this sample demonstrate that, for all temperatures $T < T_{C1}$, the total volume of FM phases (FMI and FMM) remains practically unchanged. On the other hand, a considerable splitting between FC and ZFC curves below T_{C1} (see Fig. 1), indicates the existence of a spin/cluster-glass-like state. Thus, only the (b) and (c) scenarios should be taken into account. Within the temperature range 120 K $< T < T_{C1}$ the FMM phase is the main contributor to the EMR signal. This signal sharply decreases in intensity and shifts rapidly toward zero H at low temperatures. At $T < 120$ K some part of the resonant FMM absorption plausibly turns to a non-resonant one, which causes the reduction of the integral intensity of the entire EMR spectrum. However, there are several temperature points upon approaching T_{max}, where most of the FMM signal remains within the integration interval. Since the DIN reduction was also observed at these points [see Fig. 10(a)] one may conclude that the spin/cluster glass effect also plays an important role in the DIN reduction observed.

The temperature dependences of H_r reflect changes in the magnetic anisotropy. The absolute value of the EMR signal shift from its $g = 2$ position is proportional to the ratio of effective constant of the corresponding magnetocrystalline anisotropy to magnetization. With decreasing temperature the FMI phase EMR signal shifts toward high fields—see Fig. 9. However, within the investigated temperature region, the magnetization remains practically unchanged. Thus one can suppose that the magnetic anisotropy of the FMI phase increases upon decreasing temperatures. The same conclusion may be drawn for the FMM phase, where shift of the FMR line vs temperature also reflects the change of its magnetic anisotropy parameter—see Fig. 9. The above conclusions are in line with the results of magnetic measurements, given in Fig. 4.

In summary, a number of experiments involving measurements of electrical resistance, magnetization and EMR were employed in our study of magnetic and transport properties of $Pr_{0.8}Ca_{0.2}MnO_3$ crystal. Two ferromagnetic transitions were observed at $T_{C1} \approx 130$ K and $T_{C2} \approx 60$ K, designate long range ordering of Mn and Pr spins, respectively. Both of transitions demonstrates an opposite noticeable pressure coefficient $dT_{C1}/dP \approx 0.24$ K/kbar and $dT_{C2}/dP \approx -0.75$ K/kbar. The angular dependence of the magnetization in the (110) plane exhibits a twofold symmetry anisotropy. The anisotropy field H_A in (100) plane increases approximately linearly at decreasing temperatures and approaches approximately a value of 12 kOe, at $T = 80$ K. A rise of the anisotropy field under pressure has been observed as well. The resistivity $\rho(T)$ obeys the Arrhenius law at 140 K$\leq T \leq$ 300 K with an activation energy $E_a = 130$ meV, while below T_{C1} $E_a = 60$ meV. The change in the activation energy is presumably associated with the transformation of phonon spectra and band structure attributed to the anomalies of lattice parameters, near T_{C1}. The MR vs magnetic field dependence changes from a bell-shaped form at T

$>T_{C1}$ to an almost linear dependence at $T<T_{C1}$, and approaches a maximal value of about 25% near T_{C1} for $H = 14.5$ kOe. The dynamic resistivity R_d exhibits a pronounced dependence on a bias current above and below T_{C1}. For example, a bias current of 100 μA at $T = 150$ K decreases R_d by 10%. The application of such a current at $T = 90$ K results in a fourfold reduction of the R_d. A higher magnetic anisotropy and localization effects occur in the $Pr_{0.8}Ca_{0.2}MnO_3$ single crystal with respect to $La_{1-x}Ca_xMnO_3$ crystals having a similar level of doping. This may be attributed to higher orthorhombic strain and to the formation of an orbital ordered state. EMR provides the most clear cut indication on phase separation in $Pr_{0.8}Ca_{0.2}MnO_3$: below T_{C1} two resonance lines assigned to FMI and FMM phases are clearly observed. The EMR signal intensity above $1.2\,T_{C1}$ follows the Arrhenius equation with

two activation energies, alternating at $T \sim 200$ K. Possible mechanisms, such as the destabilization of the OO and the motion of charge/spin density wave condensate for current induced suppression of the dynamic resistance in the ferromagnetic state are discussed.

ACKNOWLEDGMENTS

[1] *Colossal Magnetoresistive Oxides*, edited by Y. Tokura (Gordon and Breach Science Publishers, New York, 2000).

[2] E. Dagotto, T. Hotta, and A. Moreo, Phys. Rep. **344**, 1 (2001).

[3] J. B. Goodenough, Aust. J. Phys. **52**, 155 (1999).

[4] A. J. Millis, P. B. Littlewood, and B. I. Shraiman, Phys. Rev. Lett. **74**, 5144 (1995).

[5] C. Martin, A. Maignan, M. Hervieu, and B. Raveau, Phys. Rev. B **60**, 12 191 (1999).

[6] Z. Jirak, S. Krupicka, Z. Simsa, M. Dlouha, and S. Vratislav, J. Magn. Magn. Mater. **53**, 153 (1985).

[7] V. Kiryukhin, D. Casa, J. P. Hill, B. Keimer, A. Vigliante, Y. Tomioka, and Y. Tokura, Nature (London) **386**, 813 (1997).

[8] M. Fiebig, K. Miyano, Y. Tomioka, and Y. Tokura, Science **280**, 1925 (1998).

[9] K. Ogawa, W. Wei, K. Miyano, Y. Tomioka, and Y. Tokura, Phys. Rev. B **57**, R15033 (1998).

[10] Y. Moritomo, H. Kuwahara, Y. Tomioka, and Y. Tokura, Phys. Rev. B **55**, 7549 (1997).

[11] A. Asamitsu, Y. Tomioka, H. Kuwahara, and Y. Tokura, Nature (London) **388**, 50 (1997).

[12] A. Wahl, V. Hardy, C. Martin, and Ch. Simon, Eur. Phys. J. B **26**, 135 (2002).

[13] S. Mercone, A. Wahl, Ch. Simon, and C. Martin, Phys. Rev. B **65**, 214428 (2002).

[14] A. Wahl, Ch. Simon, S. Mercone, D. Saurel, and C. Martin, cond-mat/0206073 (unpublished).

[15] V. Markovich, I. Fita, R. Puzniak, M. I. Tsindlekht, A. Wisniewski, and G. Gorodetsky, Phys. Rev. B **66**, 094409 (2002).

[16] A. I. Shames, E. Rozenberg, W. H. McCarroll, M. Greenblatt, and G. Gorodetsky, Phys. Rev. B **64**, 172401 (2001).

[17] V. Markovich, E. Rozenberg, A. I. Shames, G. Gorodetsky, I. Fita, K. Suzuki, R. Puzniak, Y. M. Mukovskii, and D. Shulyatev, Phys. Rev. B **65**, 144402 (2002).

[18] J. Dho, E. O. Chi, N. M. Hur, K. W. Lee, H. S. Oh, and Y. N. Choi, Solid State Commun. **123**, 441 (2002).

[19] M. T. Causa, M. Tovar, A. Caniero, F. Prado, G. Ibañez, C. A. Ramos, B. Alascio, X. Obradoros, S. Piñol, Y. Tokura, and S. B. Oseroff, Phys. Rev. B **58**, 3233 (1998).

[20] A. Shengelaya, Guo-meng Zhao, H. Keller, K. A. Müller, and B. I. Kochelaev, Phys. Rev. B **61**, 5888 (2000).

[21] D. L. Huber, G. Alejandro, A. Caniero, M. T. Causa, F. Prado, M. Tovar, and S. B. Oseroff, Phys. Rev. B **60**, 12 155 (1999).

[22] T. Mizokawa, D. I. Khomskii, and G. A. Sawatsky, Phys. Rev. B **63**, 024403 (2001).

[23] M. V. Zimmermann, C. S. Nelson, J. P. Hill, D. Gibbs, M. Blume, D. Casa, B. Keimer, Y. Murakami, C.-C. Kao, C. Venkataraman, T. Gog, Y. Tomioka, and Y. Tokura, Phys. Rev. B **64**, 195133 (2001).

[24] J. A. Alonso, M. J. Martinez-Lope, M. T. Casais, and M. T. Fernandez-Diaz, Inorg. Chem. **39**, 917 (2000).

[25] J. Rodriguez-Carvajal, M. Hennion, F. Moussa, A. H. Moudden, L. Pinsard, and A. Revcolevschi, Phys. Rev. B **57**, R3189 (1998).

[26] D. Sanchez, J. A. Alonso, and M. J. Martinez-Lope, J. Chem. Soc. Dalton Trans. **23**, 4422 (2002).

[27] I. Solovyev, N. Hamada, and K. Terakura, Phys. Rev. Lett. **76**, 4825 (1996); K. Terakura, I. V. Solovyev, and N. Hamada, in *Colossal Magnetoresistive Oxides*, edited by Y. Tokura (Gordon and Breach Science Publishers, New York, 2000).

[28] M. Roy, J. F. Mitchell, A. P. Ramirez, and P. Schiffer, Phys. Rev. B **62**, 13 876 (2000); M. Roy, J. F. Mitchell, A. P. Ramirez, and P. Schiffer, Philos. Mag. B **81**, 417 (2001).

[29] T. Penney, M. W. Shater, and J. B. Torrance, Phys. Rev. B **5**, 3669 (1972).

[30] Y. Yuzhelevski, V. Markovich, V. Dikovsky, E. Rozenberg, G. Gorodetsky, G. Jung, D. A. Shulyatev, and Ya. M. Mukovskii, Phys. Rev. B **64**, 224428 (2001).

[31] Y. Tokura and N. Nagaosa, Science **288**, 462 (2000).

[32] N. Kida and M. Tonouchi, Phys. Rev. B **66**, 024401 (2002).

[33] G. Gruner, Rev. Mod. Phys. **60**, 1129 (1988).

[34] J. B. Goodenough, Struct. Bonding (Berlin) **98**, 1 (2001).

[35] A. Butera, A. Fainstein, E. Winkler, J. van Tol, S. B. Oseroff, and J. Tallon, J. Appl. Phys. **89**, 7666 (2001).

[36] D. N. H. Nam, K. Jonason, P. Nordblad, N. V. Khiem, and N. X. Phuc, Phys. Rev. B **59**, 4189 (1999).